Optical microcirculatory skin model: assessed by Monte Carlo simulations paired with *in vivo* laser Doppler flowmetry

Ingemar Fredriksson
Marcus Larsson
Tomas Strömberg
Linköping University
Department of Biomedical Engineering
University Hospital
S-581 85 Linköping, Sweden

Abstract. An optical microvascular skin model, valid at 780 nm, was developed. The model consisted of six layers with individual optical properties and variable thicknesses and blood concentrations at three different blood flow velocities. Monte Carlo simulations were used to evaluate the impact of various model parameters on the traditional laser Doppler flowmetry (LDF) measures. A set of reference Doppler power spectra was generated by simulating 7000 configurations, varying the thickness and blood concentrations. Simulated spectra, at two different source detector separations, were compared with *in vivo* recorded spectra, using a nonlinear search algorithm for minimizing the deviation between simulated and measured spectra. The model was validated by inspecting the thickness and blood concentrations that generated the best fit. These four parameters followed *a priori* expectations for the measurement situations, and the simulated spectra agreed well with the measured spectra for both detector separations. Average estimated dermal blood concentration was 0.08% at rest and 0.63% during heat provocation (44 °C) on the volar side of the forearm and 1.2% at rest on the finger pulp. The model is crucial for developing a technique for velocity-resolved absolute LDF measurements with known sampling volume and can also be useful for other bio-optical modalities.
[DOI: 10.1117/1.2854691]

Keywords: laser Doppler velocimetry; simulations; biomedical optics; Doppler effect; multiple scattering; optical properties.

Paper 07242R received Jul. 6, 2007; revised manuscript received Sep. 13, 2007; accepted for publication Sep. 29, 2007; published online Feb. 28, 2008.

1 Introduction

Laser Doppler flowmetry (LDF) is an established technology that is used to quantify temporal or spatial variations in microcirculatory blood perfusion. The technique is based on the frequency change, or Doppler shift, that occurs when light is scattered by a moving object. In human tissue, the amount and magnitude of the quasi-elastic light scattering events that take place depend on the concentration and velocity of red blood cells (RBCs). However, as a result of the optical turbidity and random direction of the blood vessels, a distribution of Doppler frequencies can be expected, even if the tissue is perfused only by a single blood flow velocity. The relationship between the distribution of Doppler frequencies and flow velocity is further complicated by multiple Doppler shifts, homodyne detection, and the complex interaction between propagating photons and static scatterers and absorbers (sampling volume). In classical LDF setups, these issues are overlooked while a single perfusion value is calculated from the detected distribution of Doppler frequencies. Consequently, this perfusion measure only reflects relative variations in the average blood concentration and flow velocity with no information on the sampling volume or depth, and intra- and interindividual comparisons are troublesome. By introducing an optical model for photon transport simulations, using tissue-relevant properties, these obstacles could be addressed, opening up new possibilities for velocity-resolved absolute LDF measurements with known sampling volumes.

The human skin is a highly heterogeneous tissue that consists of different layers and microvascular blood vessels, making it difficult to model accurately. Optical models that include many of these structures have previously been presented by Meglinski and Matcher[1] and Tuchin.[2] However, these models are inadequate for modeling Doppler spectra, as they lack information on the RBC concentration[2] and/or velocity.[1] The validation with diffuse reflectance spectroscopy of the former model is questionable due to the assumption of a wavelength-independent scattering coefficient and extremely high water absorption,[1] whereas, the latter is not validated at all using *in vivo* measurement.[2]

The aim of this study is to present a skin model with geometrical and optical properties (at 780 nm) from the current literature, based on the models mentioned above.[1,2] Emphasis

Address all correspondence to Ingemar Fredriksson, Linköping University, Dept. of Biomedical Engineering, University Hospital, S-581 85 Linköping, Sweden; Tel: 46 13 222483; Fax: 46 13 101902; E-mail: ingfr@imt.liu.se.

1083-3668/2008/13(1)/014015/12/$25.00 © 2008 SPIE

is put on the different blood layers and the distribution of RBCs moving with three representative velocities (0.3, 3.0, and 30 mm/s) within the layers. The skin model includes four varying parameters: a general skin layer thickness-scaling factor and the three concentrations of blood of different flow velocities. The model is validated by recording Doppler power spectra from a probe-based LDF system with two source-detector fiber separations (0.25 and 1.2 mm). Baseline measurements are carried out on forearm and finger pulp skin and heat provocations on forearm skin. Measured Doppler power spectra are compared to Monte Carlo simulated spectra. The skin model is considered valid (1) if there exists a set of parameters that yields simulated spectra for the two fiber distances that agree with measured spectra, and (2) if the parameters agree with *a priori* expectations during the baseline measurements (higher concentration of blood and thicker skin in the finger pulp) and the heat provocation (increased blood concentration especially for high velocities).

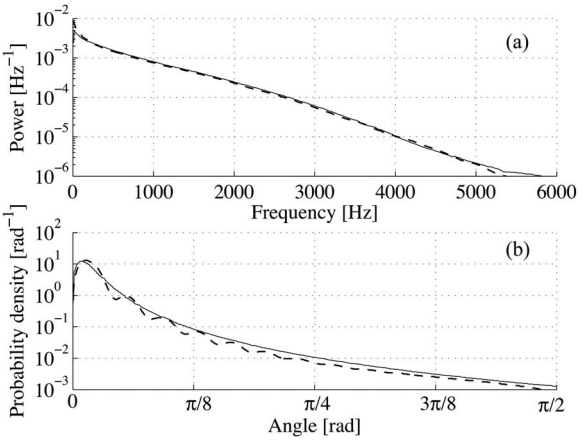

Fig. 1 (a) Comparison of the Doppler power spectrum from measurements on whole blood flowing in a plastic tube (solid line) and a Monte Carlo simulation (dashed line) using the optimal Gegenbauer kernel phase function, with α_{Gk}=1.0 and g_{Gk}=0.948, giving an anisotropy of 0.991. (b) Optimal Gegenbauer kernel phase function (solid line) and a Mie phase function (dashed line) where the red blood cells were approximated to spheres, giving an anisotropy factor of 0.993.

2 Materials and Methods

2.1 *Skin Model*

The proposed model, valid at 780 nm, is divided into six semi-infinite flat layers approximating the anatomical structure of the skin,[3] similar to the models developed by Meglinski and Matcher[1] and Tuchin.[2] The various layers—epidermis, papillary dermis, superior blood net, reticular dermis, inferior blood net, and subcutis—differ in optical properties, thickness, and blood concentration at three different flow velocities.

2.1.1 *Optical properties*

The top layer, epidermis, contains no blood but is highly absorbent due to melanin. According to Jacques,[4] the absorption coefficient μ_a (mm^{-1}) of melanin can be approximated to

$$\mu_a^{mel}(\lambda) = 6.6 \times \lambda^{-10/3} \times 10^{10}, \quad (1)$$

where λ is the wavelength (nm). For 780 nm, this yields an absorption coefficient of 15 mm^{-1}. Apart from the melanin, the epidermis, as well as the other skin layers, has a generic absorption coefficient caused by other components in the skin.[4] This generic absorption is approximated to 0.1 mm^{-1} at 780 nm, based on Salomatina et al.;[5] a value that is well in line with most of the values presented by Mobley and Vo-Dinh.[6] The total absorption coefficient of the epidermis is calculated as the sum of the generic absorption coefficient and the melanin absorption coefficient weighted by its concentration, set to 2% for fair Caucasian skin. All tissues contain a large fraction of water, which also absorbs light. However, the water absorption is not a part of this model because its absorption coefficient[7] is only about 0.002 mm^{-1} at 780 nm, which is well below the generic absorption coefficient of 0.1 mm^{-1}.

The skin contains scattering structures, especially large collagen fibers scattering in the Mie regime, and small cell structures scattering in the Rayleigh regime.[4] The reduced scattering coefficient μ_s' (mm^{-1}) for epidermis, dermis, and subcutis has been measured by Salomatina et al. over a wide wavelength range.[5] At 780 nm, the results were 3.5 mm^{-1} for epidermis and 2.0 mm^{-1} for dermis and subcutis. Assuming an anisotropy factor g of 0.85,[1,2,8] this results in a scattering coefficient μ_s of 23 mm^{-1} for epidermis and 13 mm^{-1} for dermis and subcutis, which is well in line with Jacques[4] and Graaff et al.,[9] and most of the values presented by Mobley and Vo-Dinh.[6]

The refractive index n of all skin layers, as well as for blood, is set to 1.40 in the model. This is done to avoid

Table 1 Optical properties of melaninless and bloodless skin, blood, and melanin at 780 nm. Dermis reaches from the papillary dermis to the deep blood net. Note that the refractive index n is set to 1.40 to avoid Fresnel reflections at the distinct borders between the layers.

Tissue Type	n (-)	μ_a (mm^{-1})	μ_s' (mm^{-1})	μ_s (mm^{-1})	g (-)
Melaninless epidermis	1.40	0.1	3.5	23	0.85
Bloodless dermis	1.40	0.1	2.0	13	0.85
Bloodless subcutis	1.40	0.1	2.0	13	0.85
Blood	1.40	0.5	2.0	222	0.991
Melanin	—	15	—	—	—

Table 2 Various types of vessels, their total cross-sectional area, and their average velocity (see Ref. 19).

Vessel Type	Area (cm^2)	$\langle v \rangle$ (mm/s)
Aorta	2.5	330
Small arteries	20	40
Arterioles	40	20
Capillaries	2500	0.3
Venules	250	3.3
Small veins	80	10
Venae cavae	8	100

Fresnel reflections in the anatomically incorrect perfectly parallel borders between the layers.

The optical properties of whole blood (42% hematocrit) are essential to the dynamic scattering that produces Doppler shifts in the skin model. The anisotropy factor of heparinized whole blood was estimated using a technique previously described by Kienle et al.,[10] using a 1.6-mm diameter polythene tube placed 1.7 mm below the surface of a piece of white polyacetal plastic, Delrin. The least-squares fit between the median Doppler power spectrum of the measurements and a Monte Carlo simulation of the same setup, was achieved for a Gegenbauer kernel phase function with $\alpha_{Gk}=1.0$ and $g_{Gk}=0.948$, giving an anisotropy factor of 0.991 [Fig. 1(a)]. This agrees well with values reported by Roggan et al.[11] and Enejder et al.[12] Furthermore, the value is not far from Mie calculations of spheres with a size distribution according to Hammer et al.[13] and refractive index of 1.40 and 1.34 for the red blood cells and blood plasma, respectively [Fig. 1(b)]. The Mie calculations yield an anisotropy factor of 0.993.

The Mie calculations above also give a reduced scattering coefficient for whole blood of 2.0 mm^{-1}, which is in good agreement with other sources.[11,12,14–16] Together with the anisotropy factor of 0.991, this yields a scattering coefficient of 222 mm^{-1}. To complete the picture of the optical properties of whole blood at 780 nm, the absorption coefficient for highly oxygenated blood is approximated to 0.50 mm^{-1}.[11,12,14,15,17] This value is rather independent of the level of oxygenation of the blood because the chosen wavelength is close to the 800-nm isosbestic point of oxygenated and deoxygenated hemoglobin.[18] A summary of the optical properties of the various skin layers, blood, and melanin is shown in Table 1.

2.1.2 *Blood flow and layer thickness*

The blood flow velocity (mm/s) varies depending on the vessel type. On average, the flow velocity is inversely proportional to its total cross-sectional area. Thus, although the cross-sectional area of each capillary is small, the total cross-sectional area of all capillaries is larger than for any other type of vessel, and, consequently, their average flow velocity is the lowest. The total cross-sectional area for various types of vessels and their approximate average flow velocity are summarized in Table 2. The values originate from Guyton[19] and the mean capillary velocity agrees with Stücker et al.[20]

Blood concentrations for three different flow velocities, or velocity components, are defined in the skin model: 0.3, 3.0, and 30 mm/s. In the standard configuration, the overall skin concentration of blood of the low velocity component is 10 times the concentration of the middle velocity component, which in turn is 10 times the concentration of the highest velocity component. This concentration distribution generates equal perfusions (concentration × velocity) for all three velocity components, which is a reasonable first assumption. The low velocity component is assumed to primarily consist of capillary flow, and this is the only velocity component in the papillary dermis layer, a layer which is known to only contain capillaries.[3] The middle velocity component is assumed to foremost consist of flow in venules, small veins, and small arterioles, whereas the high velocity component is assumed to mainly consist of large arterioles, veins, and arteries. The inferior blood net layer is a blood net at the border between the dermis and subcutis that contains many large vessels. Therefore, the concentration of the high velocity component is relatively high in this layer. The blood concentrations[4,21] of each layer in the standard configuration are shown together with the melanin content[4,21] and the thickness[1–5,21–23] of each layer in Table 3.

Table 3 The six skin layers and their thickness, melanin concentration, and blood concentration for the three different velocity components, 0.3, 3.0, and 30 mm/s.

			c_{blood} (%)		
Layer	t (mm)	c_{mel} (%)	0.3 mm/s	3.0 mm/s	30 mm/s
Epidermis	0.075	2.0	0	0	0
Papillary dermis	0.15	0	0.2	0	0
Superior blood net	0.15	0	0.6	0.05	0.001
Reticular dermis	0.80	0	0.1	0.01	0.0006
Inferior blood net	0.40	0	0.25	0.035	0.006
Subcutis	10	0	0.1	0.01	0.001

2.2 *Monte Carlo Simulations*

Various configurations of the skin model described in Sec. 2.1 were simulated using an in-house developed Monte Carlo software. The software is based on Prahl et al.[24] and validated to Wang et al.,[25] with an extended functionality for simulating Doppler shifts.[26] The source and detector in the simulations were configured to mimic the probe described in Sec. 2.3, making use of the rotational symmetry.[27] In the layers containing blood, it was decided at each scattering occasion if the photon was to be scattered by the static matrix or by a RBC, thus causing a Doppler shift. The decision was based on the concentration of blood, the scattering coefficient of the blood and the static matrix, respectively. The Doppler shift f_D of each RBC scattering event was calculated according to

$$f_D = -\frac{\mathbf{v}\cdot\mathbf{q}}{2\pi} = -v\frac{2}{\lambda}\cos\alpha\cos\varphi\sin(\theta/2), \tag{2}$$

where $\mathbf{v}$ is the velocity vector of the moving RBC, and $\mathbf{q}$ is the scattering vector defined as $\mathbf{q}=\mathbf{k_i}-\mathbf{k_s}$, where $\mathbf{k_i}$ and $\mathbf{k_s}$ are the circular wave number vectors for the incident and scattered photons, respectively. Furthermore, λ is the wavelength, α is the angle between $\mathbf{v}$ and the plane of scattering, φ is the angle between $\mathbf{q}$ and $\mathbf{v}$, and θ is the scattering angle dependent on the anisotropy factor g.[28] Three different blood flow components, with an average flow velocity of 0.3, 3.0, and 30 mm/s, respectively, were defined for each layer. The actual component responsible for producing the Doppler shift was randomly chosen among these components, based on the relative amount present of each of them. The actual velocity v was then randomly chosen from a rectangular distribution between 0 and twice the mean velocity of the scattering blood component, mimicking a parabolic flow profile. A random blood flow direction was assumed.

The optical Doppler spectrum, $I(f)$, for the two source-detector separations, was calculated as the distribution of accumulated frequency shifts for the detected photons. The Doppler power spectrum $P(f)$ was calculated as the autocorrelation of the optical Doppler spectrum[28]

$$P(f) = I \star I(f). \tag{3}$$

As a Doppler power spectrum has the approximate shape af^{-b} ($b>0$), the power at high frequencies is generally a couple of decades lower than the power at low frequencies. Therefore, a variance reduction method,[29] especially suited for higher Doppler frequencies, was developed. When the first Doppler scattering occasion of a photon was registered, the photon was split into 50 new photons, each having 1/50 of the weight of the original photon. Each of these new photons was then scattered in random directions causing different Doppler shifts. At successive Doppler scattering occasions, a photon was split again in two new photons if the total frequency shift of the photon exceeded $n\times 10/6$ kHz ($n=1,2,\ldots,6$). Thus, each photon was split into 50 new photons at the first Doppler scattering occasion, then into two new photons when the total shift exceeded 1.67 kHz, then into two new when it exceeded 3.33 kHz, and so on up to 10 kHz. One photon could thus be split into at most $50\times 2^6=3200$ photons. This technique drastically decreased the variance, especially for high frequencies, diminishing the need for simulating many photons.

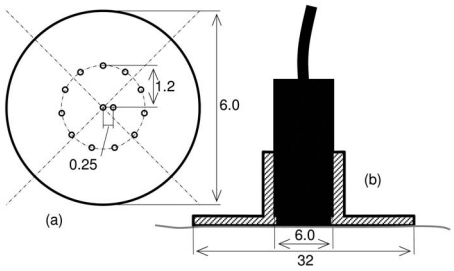

Fig. 2 Geometry of the probe tip with optical fibers at two distances from the central emitting fiber (a). Position of the probe within the probe holder and relative to the skin surface (b). Measures are in millimeters.

In the main simulation setup of the presented skin model, four different parameters were altered: the thickness and the three blood concentrations corresponding to the blood velocity components at 0.3, 3.0, and 30 mm/s. All layers were altered equally with factors relative to the standard configuration in Table 3. The alterations were made by multiplying the thickness or blood concentrations with powers of 2, so-called *dyadic factors*. The thickness was altered in 5 steps $(2^{-2},2^{-1},\ldots,2^2)$, the low and middle velocity components in 10 steps $(2^{-3},2^{-2},\ldots,2^6)$, and the high velocity component in 14 steps $(2^{-3},2^{-2},\ldots,2^{10})$. All possible combinations $(5\times 10\times 10\times 14=7000)$ were simulated. In addition, a number of configurations were simulated to examine the impact of some of the other parameters on the Doppler power spectrum. These other parameters were the melanin concentration in epidermis; the scattering coefficient of the epidermis, dermis, and subcutis; the absorption coefficient in dermis and subcutis; the scattering and absorption coefficients and the anisotropy factor of blood; and the distance between the probe and the skin surface. The simulations were halted when 200 000 Doppler shifted photons were detected, if nothing else is given.

2.3 *Measurement System*

All measurements were performed with a modified Periflux 5000 system (Perimed AB, Järfälla, Sweden) using a 780-nm laser diode. The system was connected to a custom-made probe (manufactured by Perimed AB, Fig. 2), consisting of 1 light emitting fiber and 12 light collecting fibers at two different distances from the emitting fiber. One light collecting fiber was placed 0.25 mm from the emitting fiber, and another 11 fibers were placed in a circle at a distance of 1.2 ± 0.1 mm from the emitting fiber (center-to-center distance, determined from a macro photograph). All fibers were made of silica with a core diameter of 0.125 mm and numerical aperture of 0.37. The fiber at 0.25 mm and the fibers at 1.2 mm were connected to two separate light detectors for separate signal processing of the two source-detector separations. The system was modified by Perimed AB to give two additional output signals for each separation (except the standard perfusion signal and the temperature); one *ac* signal varying with the light intensity of the speckle pattern formed on the detector, and one *dc* signal giving the total light intensity without the rapid intensity variations of the speckle pattern. The *ac* signal was bandpass filtered between 8 Hz and 20 kHz, and the *dc* signal was low-pass filtered with a cutoff frequency of 32 Hz. Both

signals were sampled at 50 kHz using a 12-bit analog to digital converter (DAQpad-6070E, National Instruments Corporation, Austin, Texas). The data were processed, using MATLAB 7.4 (Mathworks Inc., Natick, Massachusetts), resulting in two separate time-resolved sets of Doppler power spectra (Hz^{-1}), one for each separation. Each of these spectra was normalized with its corresponding dc^2-value, divided into 5-s long intervals, and averaged in each interval. A detailed description of this digital signal processing is given elsewhere by Larsson and Strömberg.[30]

The resulting Doppler power spectra were normalized with the total energy for frequency $f>0$ of the dc^2-normalized Doppler power spectra from a calibration measurement in motility standard (Perimed AB), where, due to Brownian motion, all detected photons are assumed to be Doppler shifted. Before this normalization, the Doppler power spectrum from the calibration measurement was modified to compensate for the bandpass filter and other corrupting effects. This was done by a linear extrapolation of the logarithmic spectrum down to 0 Hz, based on the 100- to 500-Hz frequency content, and up to 40 kHz, based on the 14- to 16-kHz frequency content. After this normalization, where an energy of 1.0 indicates that all photons have been Doppler shifted, the absolute levels of the Doppler power spectra from the measurements could be compared to simulations.

2.4 *Validation Measurements*

To validate the proposed skin model, measurements on 10 healthy persons, 5 male and 5 female, 25 to 40 (median 29) years old, fair Caucasian skin, were carried out. The study protocol was approved by the local ethical committee (Dnr 15-04). The test subjects were acclimatized in a room, holding a temperature of 24 °C to 26 °C, for 15 min prior to the measurements. Two types of measurements were performed: baseline measurements and heat provocation measurements. The baseline measurements were performed using fixated probe holders positioned on two different skin sites: one located on the middle of the volar side of the forearm, avoiding visible vessels, and one on the index finger pulp. The baseline measurements lasted for 30 s and were repeated three times for each location, switching position between the two probe holders between each measurement.

The PF 08-1 probe holder (Perimed AB) was used to hold the probe in a position perpendicular to the skin surface (Fig. 2) on the finger measurements; whereas, the PF 450 thermostatic probe holder (Perimed AB) was used for the forearm measurements. The probe holders and the probe were constructed to position the probe tip in level with the bottom of the probe holder, thus not generating any local pressure on the skin at the probe tip. Adhesive tape was used to attach the probe holders to the skin. The thermostatic probe holder was also used to accomplish the heat provocation. After 1 min, the probe holder was heated to 38 °C and after an additional 5 min, the probe holder was heated to 44 °C. The total measurement time was 15 min, using the same position on the forearm skin site as described above. All measurements were performed for both arms.

2.5 *Data Analysis*

In traditional LDF, the concentration of moving RBCs (*CMBC*) and the tissue blood perfusion (*perf*$\sim$*CMBC* $\times$ average velocity) are estimated from the dc^2-normalized Doppler power spectrum $P(f)$ as

$$CMBC = \int P(f)\mathrm{d}f, \tag{4}$$

and

$$perf = \int fP(f)\mathrm{d}f. \tag{5}$$

Both measures, and especially the *CMBC*, are highly nonlinear in relation to the actual concentration of moving RBCs; whereas, *perf* scales linearly to the average velocity.[28] In the data analysis of this study, the *CMBC* was calculated for $f>30$ Hz, avoiding the low-frequency region where large stochastic fluctuations can appear. However, it should be noted that a very large fraction of the energy of the Doppler power spectra is normally located in this region, often as much as 50%.

The reason that the traditional *perf* measure scales nonlinearly to the concentration is that multiple shifted photons have a total frequency shift that is less than the sum of the absolute values of all shifts, because the shifts have random signs. Thus, simulating a model where the absolute value of successive Doppler shifts is accumulated, generates a *perf* of that simulation that is truly linear to the number of Doppler shifts, which in turn is assumed to be linear to the blood concentration. The linear *perf* in Sec. 3.1 is approximated this way, by drawing a line through the points (0, 0) and the linear *perf* of the model with blood concentration factors of 2^{-3}. In that simulation, 600 000 Doppler shifted photons were detected.

The 7000 simulated variations of the skin model constituted a four-dimensional grid of pairs of spectra (short and long fiber separation, respectively). The least-squares fit between the validation measurements and simulations was iteratively searched for in this grid using the Levenberg-Marquardt algorithm, employing four-dimensional cubic interpolation to approximate the simulated spectra for the intermediate points in the grid. The chi-squared error used in the Levenberg-Marquardt algorithm was calculated as

$$\chi^2 = \chi^2_{0.25} + \chi^2_{1.2},$$

$$\chi^2_d = \frac{1}{N-1}\sum_{n=0}^{N-1}\left(1 - \frac{\langle P_{sim,d}(f_i)\rangle_{j_n\le i<j_{n+1}}}{\langle P_{meas,d}(f_i)\rangle_{j_n\le i<j_{n+1}}}\right)^2, \tag{6}$$

where $\langle\ldots\rangle$ denotes the average, d the fiber separation, f_i is the frequency of frequency bin i, and $P_{sim,d}(f_i)$ and $P_{meas,d}(f_i)$ are the Doppler power spectra of the simulation and measurement, respectively. The index j was calculated as

$$j_0 = 4,$$

$$j_i = j_{i-1} + [\sqrt{j_{i-1}}],$$

Table 4 Overview of the effect of a change of various parameters on the *perf* and *CMBC* measures for the two fiber separations. The parameters are changed from 2^{-1} times the normal value to 2^{1} times the normal value, that is 400%, except for the melanin concentration (change from 0% to 25% melanin), blood *g* (change from 0.987 to 0.995), and probe elevation (change from 0.0 to 0.2 mm). Changes of the *perf* and *CMBC* smaller than 10% are in **bold**.

Parameter	$perf_{0.25}$ (%)	$perf_{1.2}$ (%)	$CMBC_{0.25}$ (%)	$CMBC_{1.2}$ (%)
Melanin conc., norm *t* (0% to 25%)	**−8**	**+2**	**+4**	**+1**
Melanin conc., $t\times 2^2$ (0% to 25%)	−84	+18	−83	+15
Epidermis μ_s	−42	**−2**	−37	**+1**
Dermis and subcutis μ_a	−26	−29	−14	**−2**
Dermis and subcutis μ_s	+22	+12	+45	**+4**
Skin thickness	−63	−20	−52	**−1**
Blood concentration	+230	+218	+105	+22
Blood μ_a	**+5**	**+3**	**+5**	**0**
Blood μ_s	+269	+202	+107	+23
Blood *g* (0.987 to 0.995)	−39	−39	**+3**	**−1**
Probe elevation (0.0 to 0.2 mm)	−51	**−2**	−55	**−3**

$$j_{0\ldots N} < \min\begin{pmatrix} \max_j(f_j < 16\ \text{kHz}), \\ \min_j(P_{meas,d}(f_j) < 10^{-6}) \end{pmatrix}, \tag{7}$$

where […] denotes the rounding to closest integer. The indexes of *j* are denser for low frequencies than for high, making the chi-squared error more sensitive at low frequencies. This is done because the low velocity component affects a much narrower frequency interval than the middle velocity component, which in turn affects a much narrower frequency interval than the high velocity component. In this way, each velocity component affects the chi-squared error equally. It should be noted that the averaging operations in Eq. (6) effectively prevent the chi-squared error from being influenced by noise. Furthermore, the root-mean-square (RMS) error can easily be calculated from chi-squared error as

$$RMS = \sqrt{\chi^2/2}. \tag{8}$$

For each measurement, the optimization algorithm resulted in one thickness factor and three blood concentration factors, common for all layers. These factors were multiplied with the thickness and blood concentrations of the standard configuration to give an estimated thickness (mm), and three blood concentrations (vol. % blood). The thickness measure encompasses the estimated total thickness for the epidermis and the dermal layers, that is, epidermis to inferior blood net. The blood concentrations presented are the volume fraction of blood in the dermal layers, that is, papillary dermis to inferior blood net.

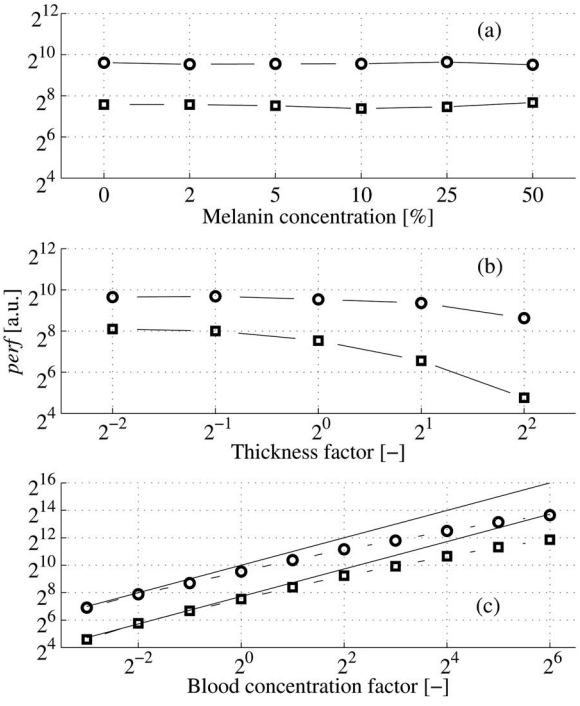

Fig. 3 Effect of melanin concentration (a), thickness (b), and blood concentration (c) changes. The circles correspond to the long fiber separation (1.2 mm) and the squares to the short (0.25 mm).

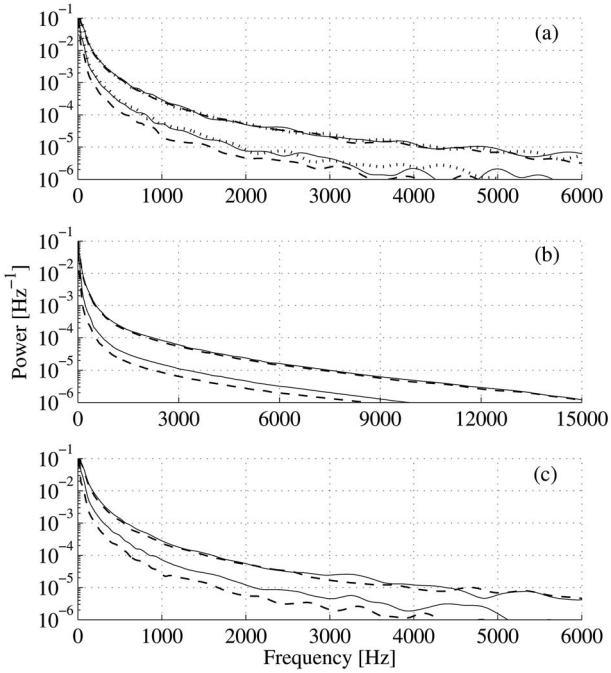

Fig. 4 (a) Simulated Doppler power spectra when the probe was positioned 0.2 mm above the skin surface (dashed lines), on the skin surface (solid lines), and on the skin surface without the extra roughness imitating layer (dotted lines). (b) As (a) but measured on the forearm. (c) Doppler power spectra from thin epidermis (2^{-1} × normal thickness, solid lines) and thick epidermis (2^{1} × normal thickness, dashed lines). The top lines originate from the long fiber separation and the lower lines from the short fiber separation in all panels.

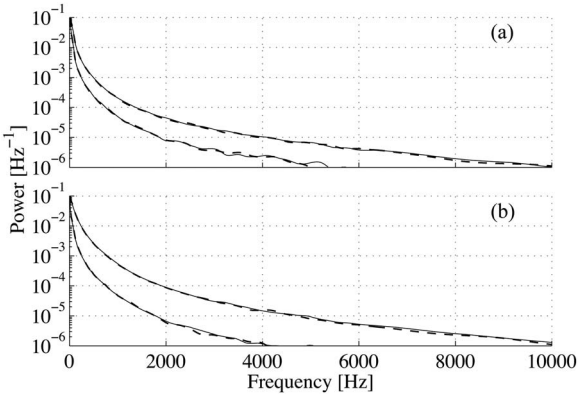

Fig. 5 Simulated (solid lines) and cubic interpolated (dashed lines) spectra for the short fiber separation (lower line pairs) and long fiber separation (top line pairs). The simulated parameters were a factor of $2^{-0.5}$ (a) and $2^{1.5}$ (b) of the standard thickness and velocity components, and the spectra were also interpolated for these points.

3 Results

3.1 *Model Parameter Influence*

The influence of various parameters of the skin model on the traditional LDF measures, *CMBC* and *perf*, was studied [Table 4]. When only the *melanin* concentration in the epidermis was changed in the standard configuration, the *CMBC* and *perf* measures were not affected [Fig. 3(a)]. The same holds true for any blood concentration and also for thinner skin, but as for thicker skin, the measures decreased drastically with melanin concentration for the short separation, whereas the measures increased with the melanin concentration for the long separation.

The short fiber separation was more sensitive to changes in the skin *thickness* (all layers), as can be seen in Fig. 3(b). It should be noted that the two thinnest configurations yield almost identical results. This was observed for all blood concentrations.

Figure 3(c) shows the effect on *perf* when all blood velocity components are changed equally. It can be seen that both measures are highly nonlinear as the concentration increases. The underestimation of *perf* relative to the linear approximation, for the highest concentration (2^6), is 72% and 80% for the short and long fiber separations, respectively. The corresponding numbers for the standard blood concentration (2^0) are 12% and 27%. The underestimation is even higher for *CMBC* as this measure cannot exceed 1.0. It can also be noted that the long fiber separation displays a greater nonlinearity than the short separation, due to a higher degree of multiple Doppler shifts.

Besides the melanin content, the thickness, and the blood concentration, parameters that are expected to differ considerably intra- and interindividually, variations between measurements in the position of the probe relative to the skin surface might occur. It was therefore investigated how the Doppler power spectra were affected by the distance between the tip of the probe and the skin surface. The skin model was slightly modified for this task to mimic the specular reflectance caused by the rough surface of the skin (not detected in the normal case when the probe tip is in contact with the skin). This was done by adding a thin (0.002 mm) highly scattering (μ_s=250 mm^{-1}, g=0) layer on top of the skin. Figure 4(a) shows the difference in the simulated Doppler power spectra when the probe was located directly on the skin surface and when it was located 0.2 mm above the surface. It should be noted that this effect for the elevated probe is not present without the extra layer, whereas that layer has no effect when the probe is located directly on the surface of the skin. Figure 4(b) shows the same effect as in Fig. 4(a), but this time from a measurement on the forearm, where the solid spectra originate from measurements where the probe was in contact with the skin, and the dashed spectra originate from measurements where the probe was positioned roughly 0.2 mm above the skin surface. For the short fiber separation, *perf* decreased from 167 to 90 in the simulation and from 248 to 150 in the measurement, when the probe was positioned 0.2 mm above the surface relative to when the probe was located directly on the skin surface. Elevating the probe in this way has the same effect as increasing the thickness of the epidermis only, which can be seen in Fig. 4(c).

It was also investigated how other parameters, expected to be constant in most measurement situations, affect the *perf* and *CMBC* measurements for the two fiber separations. This is summarized in Table 4, together with the parameters presented above.

Table 5 Interindividual mean±standard deviation of the thickness and blood concentrations for the three velocity components for all 20 measurement sites (10 persons×2 arms).

	Forearm	Finger
Thickness (mm)	1.3±0.43	2.8±0.79
$vc_{0.3}$ (%)	0.065±0.023	0.38±0.44
$vc_{3.0}$ (%)	0.013±0.007	0.33±0.21
vc_{30} (%)	0.0033±0.0017	0.53±0.41
RMS error (-)	0.19±0.02	0.18±0.07

3.2 *Interpolated Spectra*

Two simulations were carried out to study the magnitude of the error introduced by the cubic interpolation. The simulation parameters were the standard configuration times a factor of $2^{-0.5}$ for the first configuration and $2^{1.5}$ for the second, and 1 000 000 Doppler shifted photons were detected. The spectra from these simulations are shown together with the cubic interpolated spectra for these points in Fig. 5. Letting the algorithm find the parameters used in the simulations resulted in the factors $[2^{-0.50}, 2^{-0.55}, 2^{-0.50}, 2^{-0.41}]$ for the first simulation, and $[2^{1.49}, 2^{1.47}, 2^{1.55}, 2^{1.66}]$ for the second simulation. Using linear interpolation instead, the resulting factors were $[2^{-0.42}, 2^{-0.55}, 2^{-0.54}, 2^{-0.47}]$ and $[2^{1.71}, 2^{1.95}, 2^{1.62}, 2^{1.82}]$. The factors correspond to the thickness and the three velocity components, 0.3, 3.0, and 30 mm/s, respectively.

3.3 *Baseline Measurements*

The mean estimated thickness (epidermis to inferior blood net), blood concentrations for the three velocity components in dermis (papillary dermis to inferior blood net), and RMS errors for the 30-s long baseline measurements are summarized in Table 5. The standard deviations shown in that table are calculated as the standard deviation of the mean thickness and blood concentrations of the three measurements on the same site, for all 20 measurement sites for forearm and finger, respectively. For the thickness, the coefficient of variation (standard deviation/mean) between these three measurements was also calculated, and the mean of these variation coefficients was 35% for the forearm and 15% for the finger. This gives an indication of the reproducibility of the measurements. The mean estimated thickness for the forearm and finger for both arms and all test persons can be seen in Fig. 6. Figure 7 shows examples of the measured and fitted spectra for the two fiber separations for the forearm and finger, having parameters of [0.51 mm, 0.058% 0.043% 0.0020%] and [3.2 mm 0.13% 1.3% 0.26%] for the forearm and finger, respectively. The spectra having RMS errors closest to the mean errors for forearm and finger are shown.

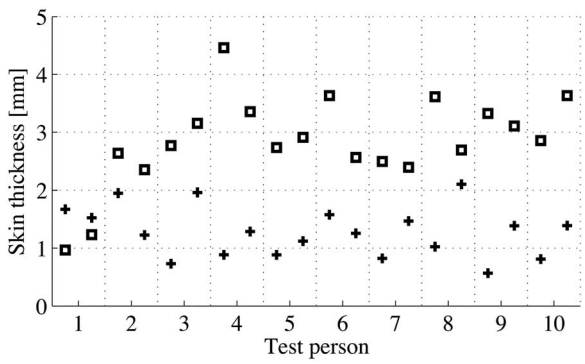

Fig. 6 Mean estimated thickness (epidermis+dermis) for all 20 measurement sites on the forearm (plus signs) and finger (squares).

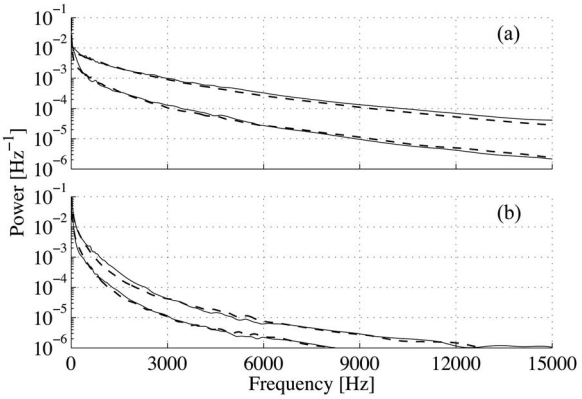

Fig. 7 Example of measured (solid lines) and simulated (dashed lines) spectra, for short fiber separation (bottom line pairs) and long fiber separation (top line pairs), for the finger (a) and forearm (b).

3.4 *Heat Provocations*

The examples shown in this section are representative, because they were chosen as the measurements with the smallest (0.11), closest-to-mean (0.17), and largest (0.22) average RMS errors. Figures 8(a) and 8(b) show the *CMBC* and *perf* from the measurement and the best-fit skin models over the whole 15-min measurement. Figure 8(c) shows the *RMS* error between the measurements and the best-fit models, and Figure 8(d) shows the estimated thickness (epidermis to inferior blood net) and the estimated blood concentrations for the three velocity components in dermis (papillary dermis to inferior blood net). Figure 9 shows examples of the Doppler power spectra at 1.0 and 14.0 min, respectively. The mean estimated thickness and blood concentration for the three velocity components in dermis at 1.0 and 14.0 min are summarized in Table 6, where the corresponding RMS errors are also shown. In general (15 cases out of 20), the estimated thickness increased during the heat provocation. The blood concentration of the low velocity component increased in 12 cases; whereas, the blood concentration of the two higher velocity components increased drastically in all cases.

4 Discussion

4.1 *Effect of Optical Properties*

The optical properties (OP) of skin are central to the model. In Sec. 3.1, it was evaluated how the OP affected the Doppler power spectra in terms of the traditional *CMBC* and *perf* measures. Theoretically, an increased energy in the Doppler power spectra (increased *CMBC* and *perf*) would increase the estimated blood concentrations; whereas, a shift of the energy

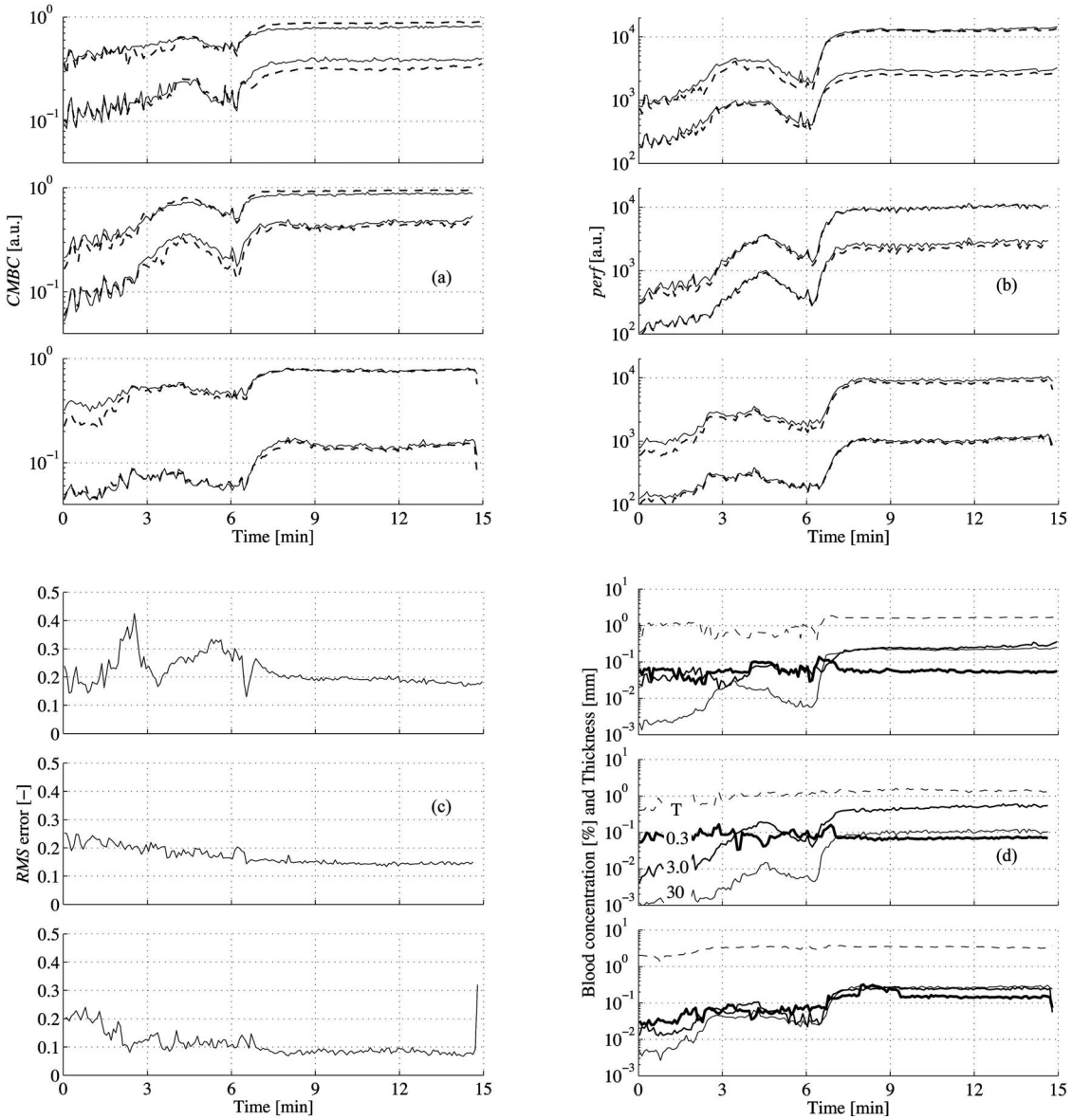

Fig. 8 Three examples of the results of the fit to the heat provocation measurements: best case (lower panels), mean case (middle panels), and worst case (upper panels), with respect to average RMS error. (a and b) *CMBC* and *perf* from measurements (solid lines) and best-fit skin model simulations (dashed lines) for short separation (lower line pairs) and long separation (upper line pairs). (c) RMS error between the measured and simulated spectra. (d) Thickness (dashed lines) and blood concentrations for the three velocities (gray thick lines—0.3 mm/s; gray thin lines—3.0 mm/s; dark thin lines—30 mm/s) for the best-fit models.

toward higher frequencies (only increased *perf*, constant *CMBC*) would shift the blood concentrations slightly toward the higher velocity components. It was shown that a change with a factor of 4 in any of the OP (not including the OP of blood) changed *CMBC* and *perf* only by a factor about 0.4 or less. Only the combination of thick skin and extreme variations in melanin concentration superseded this level. The uncertainty of the evaluated OP given in Table 1 is difficult to estimate, but differs in general less than 50% from OP presented by others. This indicates that *CMBC* and *perf* values (and Doppler power spectra) derived using the proposed model differ far less than a factor 0.4 from values generated by a "true" model where the skin OP are slightly different.

For thick skin, the melanin concentration becomes an important factor. However, thick skin is normally only located on the palms, palmar surface of the digits, and on the foot soles, where the concentration of melanin is low, even for otherwise dark pigmented skin types. Therefore, the high influence of high melanin concentrations in thick skin is a problem only in extraordinary situations.

Section 3.1 also shows how the OP of blood affects the Doppler power spectra. Because the absorption of blood is rather low at 780 nm, which is not much higher than the absorption of bloodless dermis and subcutis, a change of this parameter by a factor of 4 did not significantly change the Doppler power spectrum for the standard blood concentration.

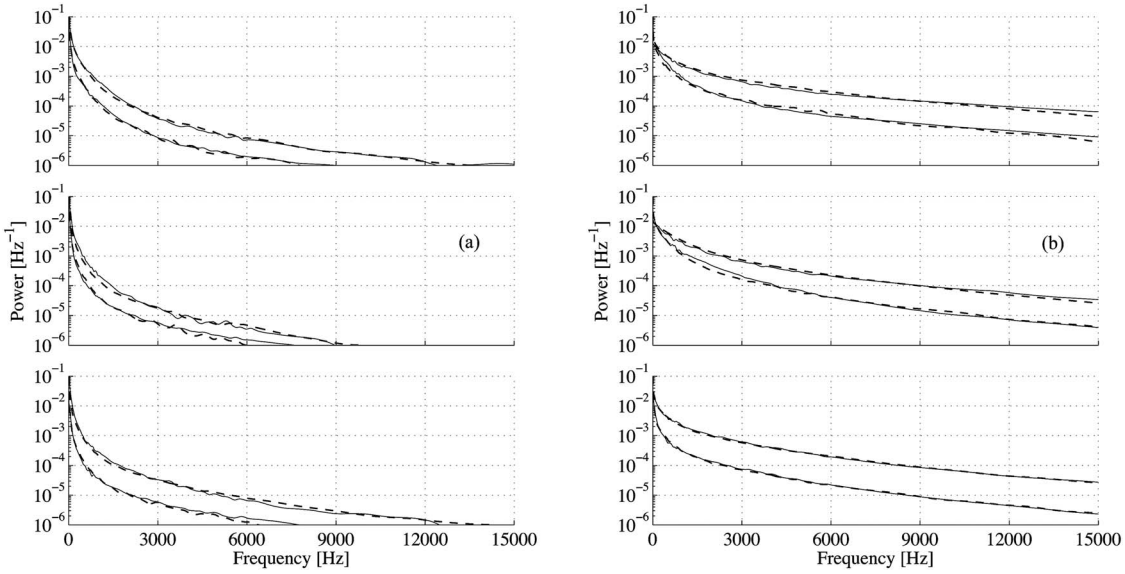

Fig. 9 Measured (solid lines) and simulated (dashed lines) Doppler power spectra at 1.0 min (a) and 14.0 min (b).

However, a small influence is expected for very high blood concentrations, as the measurement volume will decrease slightly due to a small increase in the total absorption coefficient of the dermis in that situation. On the other hand, and not surprisingly, a change in the scattering properties, that is, the scattering coefficient and the anisotropy factor g, of blood, largely affected the Doppler power spectra. A change of the scattering coefficient of blood changed the *CMBC*, and therefore also *perf*, almost at a 1:1 scale; whereas, the first momentum of the Doppler power spectrum, and therefore *perf*, is proportional to $\langle \sin(\theta/2) \rangle \approx \sin(\arccos(g)/2)$ [see Eq. (2)]. It is thus of great importance for the accuracy of the model that the scattering properties of blood given in Table 1 are accurate. It is known that the anisotropy factor is sensitive to the shape and degree of aggregation of the RBCs. Following the theoretical calculations by Enejder et al.,[12] the anisotropy factor of RBCs can vary in the range of 0.989 to 0.992, resulting in a difference in *perf* of about 15% between these two extremes.

Following the reasoning above, it can be predicted how the hematocrit of blood (set to 42% in our model) affects the results. The scattering coefficient of blood depends approximately on the hematocrit (hct) as $\mu_s = hct\,(1-hct)\,c$, where c is a constant and hct is given as a value between 0 and 1.[31] The change in μ_s is therefore much smaller than the change in hematocrit for relevant hematocrit levels. The absorption coefficient of blood changes linearly with the hematocrit, but, as previously stated, this does not affect the results significantly. The anisotropy factor is not expected to change significantly for relevant levels of the hematocrit.[12] An increase of the hematocrit will thus, due to the change of μ_s, have the same affect as a small increase of the blood concentration.

Table 6 Interindividual mean ± standard deviation of estimated thickness, blood concentrations for the three velocity components, and RMS errors at 1.0 and 14.0 min.

	t = 1.0 min	t = 14.0 min
Thickness (mm)	1.5 ± 0.8	2.2 ± 0.8
$vc_{0.3}$ (%)	0.067 ± 0.031	0.27 ± 0.35
$vc_{3.0}$ (%)	0.016 ± 0.009	0.36 ± 0.21
vc_{30} (%)	0.0037 ± 0.0019	0.15 ± 0.07
RMS error (-)	0.18 ± 0.03	0.16 ± 0.06

The chosen laser wavelength (780 nm) of the system is advantageous for several reasons. As stated above, the absorption coefficient of blood is low at that wavelength, which makes the model rather insensitive to the exact level of absorption. The fact that the absorption of blood is not much higher than the absorption of dermis, and that the reduced scattering coefficient for blood and dermis is in the same range at 780 nm, means that the measurement volume is not widely affected by variations in the blood concentration. Furthermore, the absorption coefficients are within the same range for oxygenated and deoxygenated hemoglobin at 780 nm (about 30% higher for deoxygenated hemoglobin), in contrast to for example 633 nm where the absorption of deoxygenated hemoglobin is almost 10 times higher than for oxygenated hemoglobin.[18] This makes the model insensitive to the level of oxygenation, which is also desirable. Finally, the absorption of melanin is relatively low at 780 nm, making the model less sensitive to the level of pigmentation, at least for LDF applications.

In conclusion, the OP of the static tissue had a low impact for relevant variations from the values given in Table 1. Only the scattering coefficient of blood, and thus the hematocrit level, had a substantial impact on the Doppler power spectra. However, large intra- and interindividual variations in the hematocrit level are unlikely. Consequently, the shape and magnitude of the Doppler power spectra is primarily determined

by the blood concentration and the blood flow velocity, for these two fiber separations.

4.2 *Probe Configuration*

The thickness of the skin model affected the short fiber separation (0.25 mm) to a greater extent than the long separation (1.2 mm), as observed in Fig. 3(b). Furthermore, a small change in the position of the probe above the skin surface made a larger impact on the short fiber separation, as indicated by Fig. 4. The shorter separation was also more sensitive to variations in the epidermis OP, as reported in Sec. 3.1. These findings all suggest that LDF measurements could be less sensitive to variations in the epidermis and therefore more sensitive to changes of the blood concentrations, by using longer fiber separations. This would increase the accuracy of the estimated blood concentrations using the skin model. It is also possible that longer separations could make it possible to reduce the number of layers in the model without jeopardizing the accuracy. The role of the probe configuration will therefore be further evaluated.

4.3 *Estimated Thickness*

During the measurements, it was not practically possible to control the exact position of the probe above the skin surface, and it is likely that the probe position varied between 0.0 mm and approximately 0.3 mm above the surface. This issue probably occurred more frequently during the forearm measurements as the construction of the heat probe holder made it more difficult to ensure that the probe was positioned in contact with the tissue. A small elevation of the probe above the skin surface had a high impact of the LDF readings from the short fiber separation, as seen in Fig. 4. This explains why the estimated thickness varied considerably for the three repetitive measurements on the same site, especially for the forearm measurements (variation coefficient 35% on forearm and 15% on finger). However, the estimated thickness was consistently (18 cases out of 20) higher for the finger measurements than for the forearm measurements [Fig. 6(a) and Table 5].

The thickness factor and the blood concentration factors affect all the skin layers equally. This is a weakness in the model, but having separate parameters for all layers would probably lead to a nonrobust algorithm with large fluctuations in the solutions due to overfitting. With the proposed model, the thickness factor can partly compensate for deviations from the fixated blood concentration relationship between the various layers. This is probably one reason why the estimated thickness generally changes slightly during the heat provocation measurements, as indicated by Fig. 8(d) and Table 6. In addition, the increase (15 cases out of 20) in thickness factor during these provocations might indicate that an actual swelling of the skin occurs. However, that conclusion should not be drawn from these estimations, because we must emphasize that the method is not intended to be used to estimate the thickness of the skin. The thickness factor is only there to ensure that the blood concentration factors are not affected by geometrical differences between model and tissue.

4.4 *Validation Measurements*

No gold standard exists to estimate the parameters in an optical skin model as the one presented in this article. Therefore, it is not a straightforward task to validate the accuracy of the model. However, there are a number of indications from the analysis of the measurements presented that together serve as a validation of the accuracy of the model. Foremost, there exists a set of the four parameters that, together with the static properties of the model, generate Doppler power spectra that agree well with both fiber separations, for all measurements performed. Examples of this agreement between the measurements and simulations are shown in Figs. 7 and 9. Taking into account the simplicity of the model, with only four free parameters, the RMS errors are generally low [Tables 5 and 6]. There exist many different sets of parameters that could generate an accurate Doppler power spectrum at just one fiber separation, but for two different separations, the number of unique models drastically decreases.

The estimated parameter values for each measurement are also as expected. The estimated total blood concentrations are within the expected range[4,21] (about 0.05% to 1.5%, Tables 5 and 6), with a much higher concentration in the finger pulp than in the forearm skin and much higher concentration in the provoked forearm skin than in the unprovoked. For the heat provocation measurements, the high velocity components increased more than the lowest velocity component, which can be expected as the thermoregulation is a process involving primarily larger vessels, where the capillary blood net can be partly bypassed by the arteriovenus shunts.[32] As mentioned previously, the estimated thickness of the finger pulp measurements was consistently higher than for the forearm measurements, which indicates that the thickness factor is related to tissue type.

Finally, the intraindividual variations for all measurements were low compared to the differences between finger and forearm and nonprovoked and provoked forearm. Because the test persons were all healthy, it was expected that the anatomical and physiological structure of their skin was similar, and the fact that the estimated model parameters were similar for all persons is therefore a final indication that the skin model is accurate.

5 Conclusions

A microcirculatory optical skin model with varying parameters has been presented. The parameters were assessed by Monte Carlo simulations paired with *in vivo* LDF measurements. It has been evaluated how various static parameters of the model affected the Doppler power spectra with regard to the traditional LDF measures *CMBC* and *perf*. It was possible to find a combination of the thickness of the model and blood concentrations at three different flow velocity components (0.3, 3.0, and 30 mm/s), that produced (using Monte Carlo simulations) Doppler power spectra that agreed well with measured Doppler power spectra, at two different fiber separations simultaneously. The estimated parameters corresponded to *a priori* expectations, as the skin thickness was consistently higher on the finger pulp than on the forearm, the blood concentration was higher in finger pulp than forearm skin and higher after a heat provocation than before it, and a heat provocation affected the higher velocity components more than the low ones.

The skin model presented is expected to be valid for laser Doppler applications on most skin types. This includes skin of

thin or normal thickness for all levels of pigmentation and lightly pigmented skin for all thicknesses. For the special case of thick and dark pigmented skin, the model must be adjusted for the melanin concentration. For other steady-state optical applications, such as diffuse reflectance spectroscopy, the melanin content of the epidermis becomes a more important parameter, and with that in mind, the model should be valid by adjusting the optical properties for other wavelengths. The skin is a very heterogeneous tissue, and therefore, six layers are used in this model. However, it could be possible to reduce the number of layers for larger source-detector separations, and it is also likely that a similar model for other types of tissue, such as the liver or the brain, can be made less complex.

Assuming that the estimated parameters of the skin model are correct, the model can be used to estimate the tissue perfusion in absolute units, that is ml *blood*/100 g *tissue* $\times$ mm/s, for any given measurement volume. The separation into flow velocity regions also enables a way of studying the isolated capillary activity by linking it to the low velocity component. Both these features are likely to drastically improve the clinical value of the LDF technique.

Acknowledgments

The project was supported by the Swedish Agency for Innovation Systems (VINNOVA) Center of Excellence for Non-Invasive Medical Measurements (NIMED), the NIMED Center for Biomedical Data Processing (a project funded by Linköping University and Perimed AB), and by the Swedish Research Council (Grant No. 2003-4751).

References

1. I. V. Meglinski and S. J. Matcher, "Quantitative assessment of skin layers absorption and skin reflectance spectra simulation in the visible and near-infrared spectral regions," *Physiol. Meas* **23**(4), 741–753 (2002).
2. V. Tuchin, *Tissue Optics: Light Scattering Methods and Instruments for Medical Diagnosis*, SPIE Optical Engineering Press, Bellingham, WA (2000).
3. G. J. Tortora and S. R. Grabowski, "The Integumentary system," in *Principles of Anatomy and Physiology*, pp. 140–159, John Wiley & Sons, Inc. (2000).
4. S. L. Jacques, "Skin Optics," *Oregon Medical Laser Center News* (1998), http://omlc.ogi.edu/news/jan98/skinoptics.html.
5. E. Salomatina, B. Jiang, J. Novak, and A. N. Yaroslavsky, "Optical properties of normal and cancerous human skin in the visible and near-infrared spectral range," *J. Biomed. Opt.* **11**(6), 064026 (2006).
6. J. Mobley and T. Vo-Dinh, "Optical properties of tissue," in *Biomedical Photonics Handbook*, T. Vo-Dinh, Ed., pp. 2.1–2.75, CRC Press, Boca Raton, FL (2003).
7. G. M. Hale and M. R. Querry, "Optical constants of water in the 200-nm to 200-μm wavelength region," *Appl. Opt.* **12**(3), 555–563 (1973).
8. M. J. v. Gemert, S. L. Jacques, H. J. Sterenborg, and W. M. Star, "Skin optics," *IEEE Trans. Biomed. Eng.* **36**(12), 1146–1154 (1989).
9. R. Graaff, A. C. M. Dassel, M. H. Koelink, F. F. de Mul, J. G. Aarnoudse, and W. G. Zijlstra, "Optical-properties of human dermis invitro and invivo," *Appl. Opt.* **32**(4), 435–447 (1993).
10. A. Kienle, M. S. Patterson, L. Ott, and R. Steiner, "Determination of the scattering coefficient and the anisotropy factor from laser Doppler spectra of liquids including blood," *Appl. Opt.* **35**(19), 3404–3412 (1996).
11. A. Roggan, M. Friebel, K. Dorschel, A. Hahn, and G. Muller, "Optical properties of circulating human blood in the wavelength range 400–2500 nm," *J. Biomed. Opt.* **4**(1), 36–46 (1999).
12. A. M. Enejder, J. Swartling, P. Aruna, and S. Andersson-Engels, "Influence of cell shape and aggregate formation on the optical properties of flowing whole blood," *Appl. Opt.* **42**(7), 1384–1394 (2003).
13. M. Hammer, D. Schweitzer, B. Michel, E. Thamm, and A. Kolb, "Single scattering by red blood cells," *Appl. Opt.* **37**(31), 7410–7418 (1998).
14. M. Friebel, A. Roggan, G. Muller, and M. Meinke, "Determination of optical properties of human blood in the spectral range 250 to 1100 nm using Monte Carlo simulations with hematocrit-dependent effective scattering phase functions," *J. Biomed. Opt.* **11**(3), 034021 (2006).
15. J. M. Steinke and A. P. Shepherd, "Diffusion-model of the optical absorbance of whole-blood," *J. Opt. Soc. Am. A* **5**(6), 813–822 (1988).
16. J. M. Steinke and A. P. Shepherd, "Comparison of Mie theory and the light-scattering of red blood-cells," *Appl. Opt.* **27**(19), 4027–4033 (1988).
17. L. O. Reynolds, C. Johnson, and A. Ishimaru, "Diffuse reflectance from a finite blood medium: Applications to the modeling of fiber optic catheters," *Appl. Opt.* **15**(9), 2059–2067 (1976).
18. W. G. Zijlstra, A. Buursma, and O. W. v. Assendelft, *Visible and Near Infrared Absorption Spectra of Human and Animal Haemoglobin Determination and Application*, VSP, Utrecht, Netherlands (2000).
19. A. C. Guyton, "Overview of the circulation, and medical physics of pressure, flow, and resistance," in *Textbook of Medical Physiology*, pp. 150–158, Saunders, Philadelphia (1991).
20. M. Stücker, V. Baier, T. Reuther, K. Hoffmann, K. Kellam, and P. Altmeyer, "Capillary blood cell velocity in human skin capillaries located perpendicularly to the skin surface: Measured by a new laser Doppler anemometer," *Microvasc. Res.* **52**(2), 188–192 (1996).
21. G. V. G. Baranoski and A. Krishnaswamy, "An introduction to light interaction with human skin," *RITA* **11**(1), 33–62 (2004).
22. R. R. Anderson and J. A. Parrish, "Optical properties of human skin," in *The Science of Photomedicine*, J. D. Regan and J. A. Parrish, Eds., pp. 147–194, Plenum Press, New York (1982).
23. A. Åkesson, R. Hesselstrand, A. Scheja, and M. Wildt, "Longitudinal development of skin involvement and reliability of high frequency ultrasound in systemic sclerosis," *Ann. Rheum. Dis.* **63**(7), 791–796 (2004).
24. S. A. Prahl, M. Keijzer, S. L. Jacques, and A. J. Welch, "A Monte Carlo model of light propagation in tissue," in *Dosimetry of Laser Radiation in Medicine and Biology*, G. J. Müller and D. H. Sliney, Eds., 102–111, SPIE, Bellingham, Wash. (1989).
25. L. H. Wang, S. L. Jacques, and L. Q. Zheng, "Mcml—Monte-Carlo modeling of light transport in multilayered tissues," *Comput. Methods Programs Biomed.* **47**(2), 131–146 (1995).
26. F. F. M. de Mul, M. H. Koelink, M. L. Kok, P. J. Harmsma, J. Greve, R. Graaff, and J. G. Aarnoudse, "Laser-doppler velocimetry and Monte-Carlo simulations on models for blood perfusion in tissue," *Appl. Opt.* **34**(28), 6595–6611 (1995).
27. H. Nilsson, M. Larsson, G. E. Nilsson, and N. O. T. Strömberg, "Photon pathlength determination based on spatially resolved diffuse reflectance," *J. Biomed. Opt.* **7**(3), 478–485 (2002).
28. I. Fredriksson, C. Fors, and J. Johansson, "Laser Doppler flowmetry—a theoretical framework," Department of Biomedical Engineering, Linköping University, Linköping, Sweden (2007), www.imt.liu.se/bit/ldf/ldf.
29. E. Veach, "Robust Monte Carlo methods for light transport simulation," Ph.D diss. Stanford University (1997).
30. M. Larsson and N. O. T. Strömberg, "Toward a velocity-resolved microvascular blood flow measure by decomposition of the laser Doppler spectrum," *J. Biomed. Opt.* **11**(1), 014024 (2006).
31. V. Twersky, "Absorption and multiple scattering by biological suspensions," *J. Opt. Soc. Am.* **60**(8), 1084–1093 (1970).
32. A. C. Guyton, "Body temperature, temperature regulation, and fever," in *Textbook of Medical Physiology*, pp. 797–808, Saunders, Philadelphia (1991).